A

		Liver				Bile duct	
		Liver weight (mg)	ratio of (+/-)/(+/+)	Incidence ratios of embryonic hepatitis		Ectopic hd formation	
B6	+/+	65.3±1.5		0/90	(0%)	5/28	(17.9%)
(N_{7-8})	+/-	42.6±4.4	(0.66)	55/88	(62.5%)	21/22	(95.5%)
ICR	+/+	97.7±2.5		0/33	(0%)	1/35	(2.9%)
	+/-	92.5±2.2	(0.95)	2/38	(5.2%)	13/38	(34.2%)
129_{SvJ}/B6	+/+	64.8±4.2		0/15	(0%)	0/15	(0%)
(N_{1-2})	+/-	59.3±2.1	(0.92)	0/12	(0%)	2/12	(16.7%)

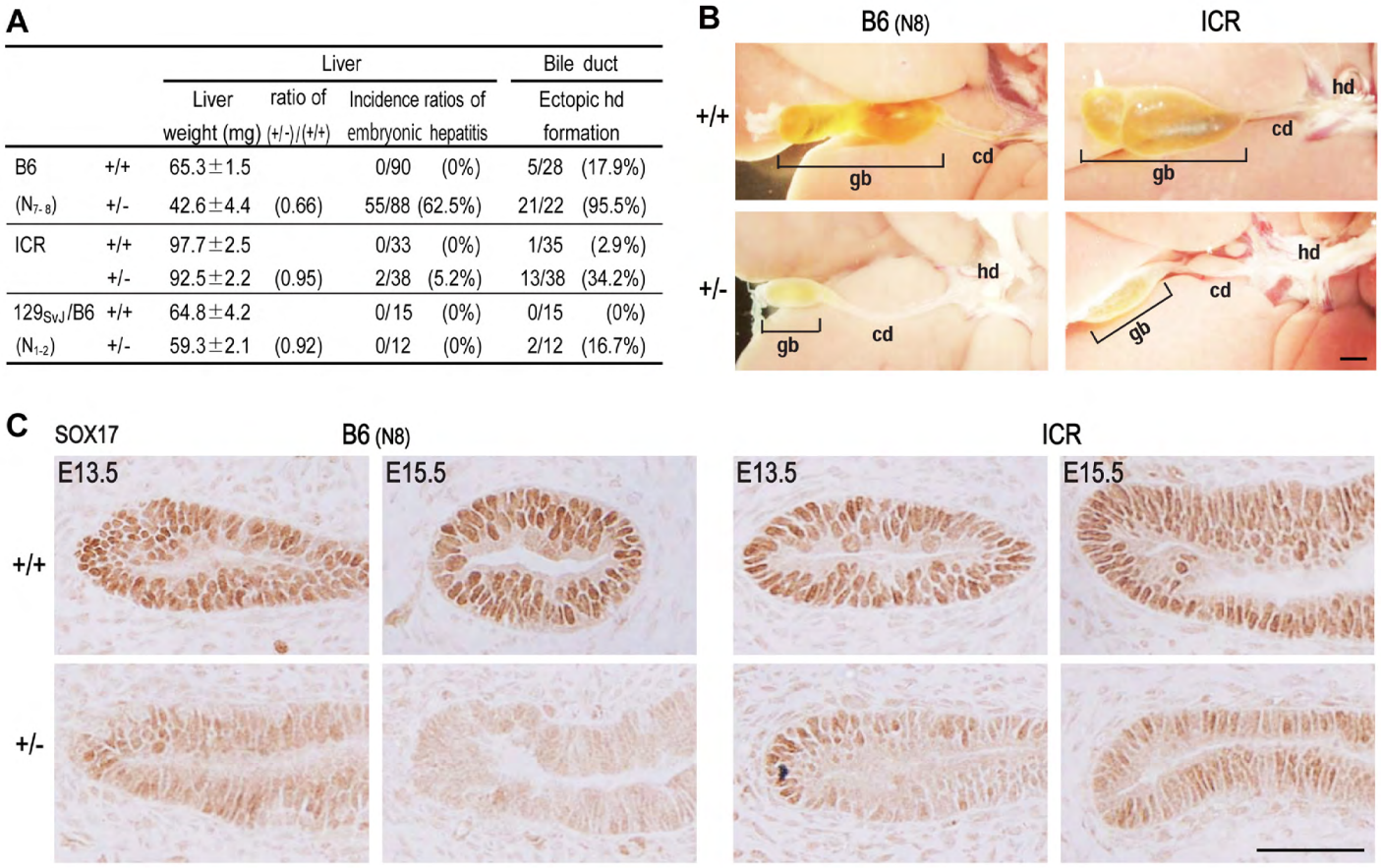

Fig. S1. Comparative phenotypes of the liver and gallbladder/bile ducts and dosage-dependent SOX17 expression in the gallbladder primordia in the *Sox17*$^{+/-}$ mice on three mixed genetic backgrounds. (**A**) Table showing comparative phenotypes [i.e. the liver weight (mg) and its ratio (*Sox17*$^{+/-}$/wild-type), and the incidence ratios of embryonic hepatitis and ectopic hepatic ducts] in the *Sox17*$^{+/-}$ embryos at 17.5 dpc on three mixed genetic backgrounds. (**B**) Gross anatomical images showing gallbladder hypoplasia at adult stage (8 weeks old) even in ICR background. The hypoplasic gallbladder in the *Sox17*$^{+/-}$ (B6) adult survivor is also shown in left lower plate. (**C**) Comparative anti-SOX17 immunostaining of the gallbladder primordia in the wild-type and *Sox17*$^{+/-}$ embryos at 13.5 and 15.5 dpc. After the gallbladder tissues were dissected from the wild-type and *Sox17*$^{+/-}$ littermates, the fixation, sectioning and staining were performed as carefully as possible under the same condition. Anti-SOX17-positive signal intensities appear to be reduced in *Sox17*$^{+/-}$ gallbladder region compared with those in wild-type counterparts in both ICR and B6 backgrounds. cd, cystic duct; hd, extrahepatic duct; gb, gallbladder. Scale bars: 1 mm in B, 50 μm in C.

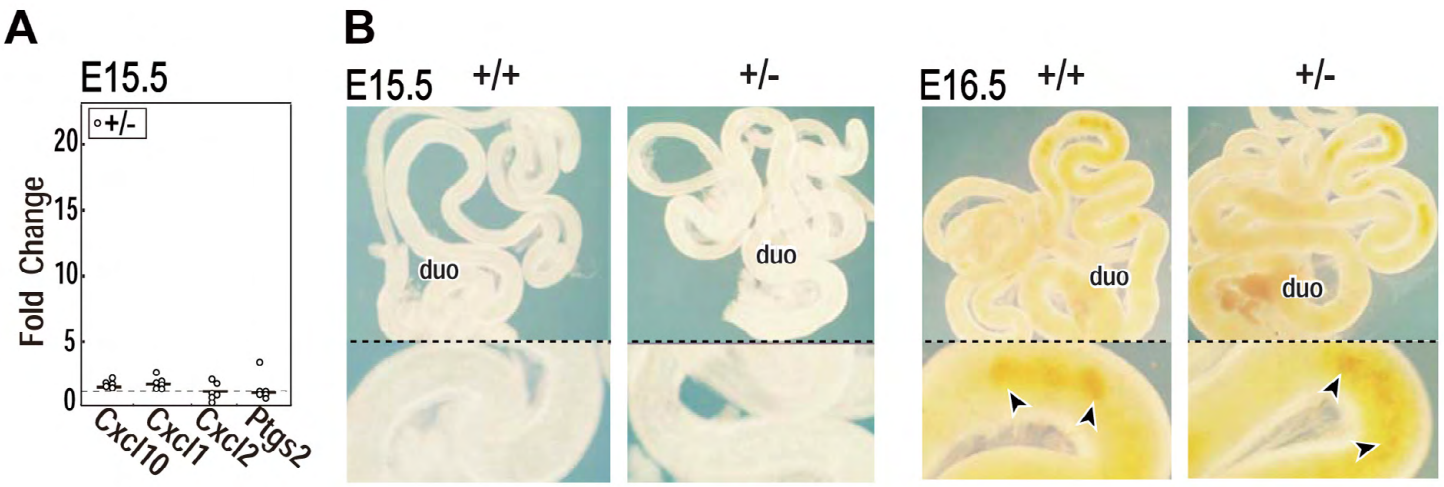

Fig. S2. No appreciable upregulation of hepatic inflammation markers in the *Sox17*$^{+/-}$ B6 livers (at 15.5 dpc) before the first biliary excretion into the fetal duodenum. (**A**) Real-time RT-PCR analysis showing normal expression levels of *Cxcl10*, *Cxcl1*, *Cxcl2* and *Ptgs2* in *Sox17*$^{+/-}$ B6 livers at 15.5 dpc. The vertical axis represents fold changes in the expression level of each liver sample relative to those of wild-type livers (the mean value was set as 1). (**B**) The gross-anatomical images of the embryonic duodenum (lower insets) and intestine before (15.5 dpc) and after (16.5 dpc) the first biliary excretion (yellow; arrowheads) into the fetal duodenum in wild-type and *Sox17*$^{+/-}$ embryos. duo, duodenum.

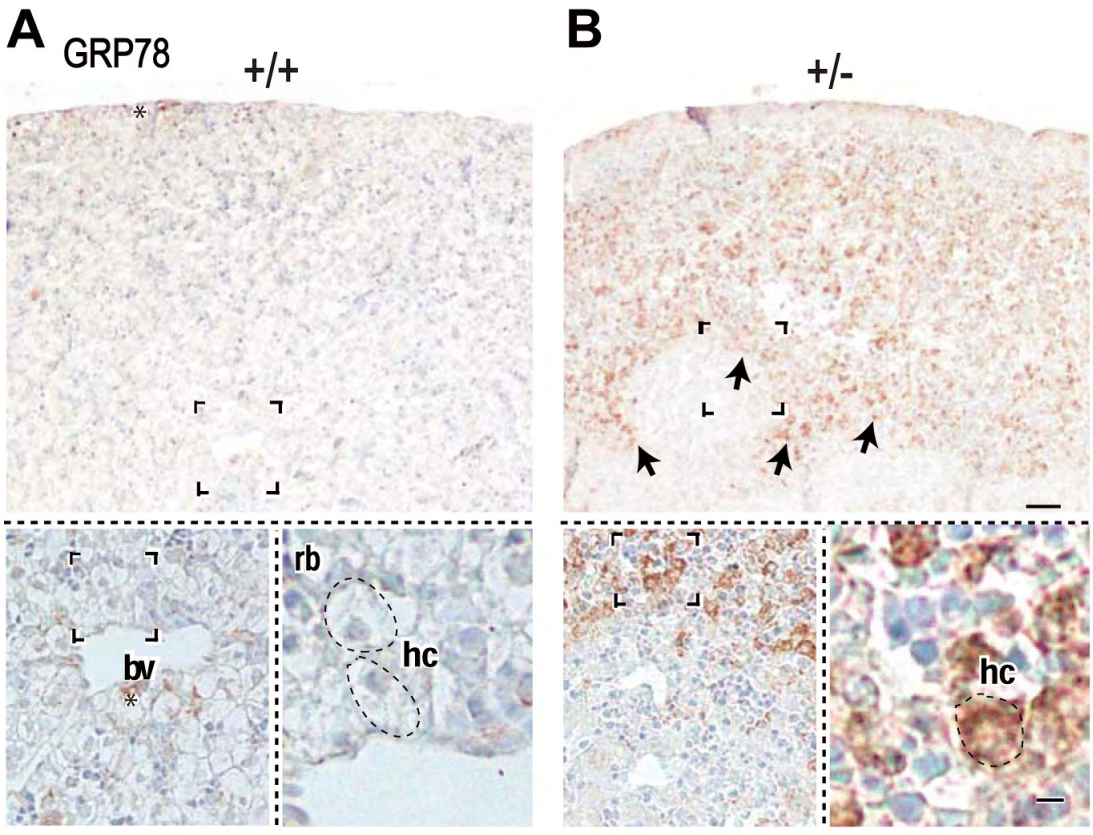

Fig. S3. Comparative anti-GRP78 immunostaining (brown) in the wild-type and *Sox17*$^{+/-}$ liver lobules. (**A**,**B**) After the liver lobules (left lateral) were dissected from the wild-type and *Sox17*$^{+/-}$ littermates at 17.5 dpc, the fixation, sectioning and staining were performed as carefully as possible under the same condition. No appreciable positive signals were detected in the wild-type liver lobules (A). GRP78-positive signals are highly detected in the hepatocytes around the degenerating peripheral region of *Sox17*$^{+/-}$ liver lobules (B, arrows). Each broken rectangle indicates the area highly magnified in the adjacent plate. asterisk, non-specific signals in the edge of the section; bv, blood vessel; hc, hepatocyte, rb, red blood (hematopoietic) cells. Scale bars: 50 μm in upper panel; 5 μm in lower-right inset.

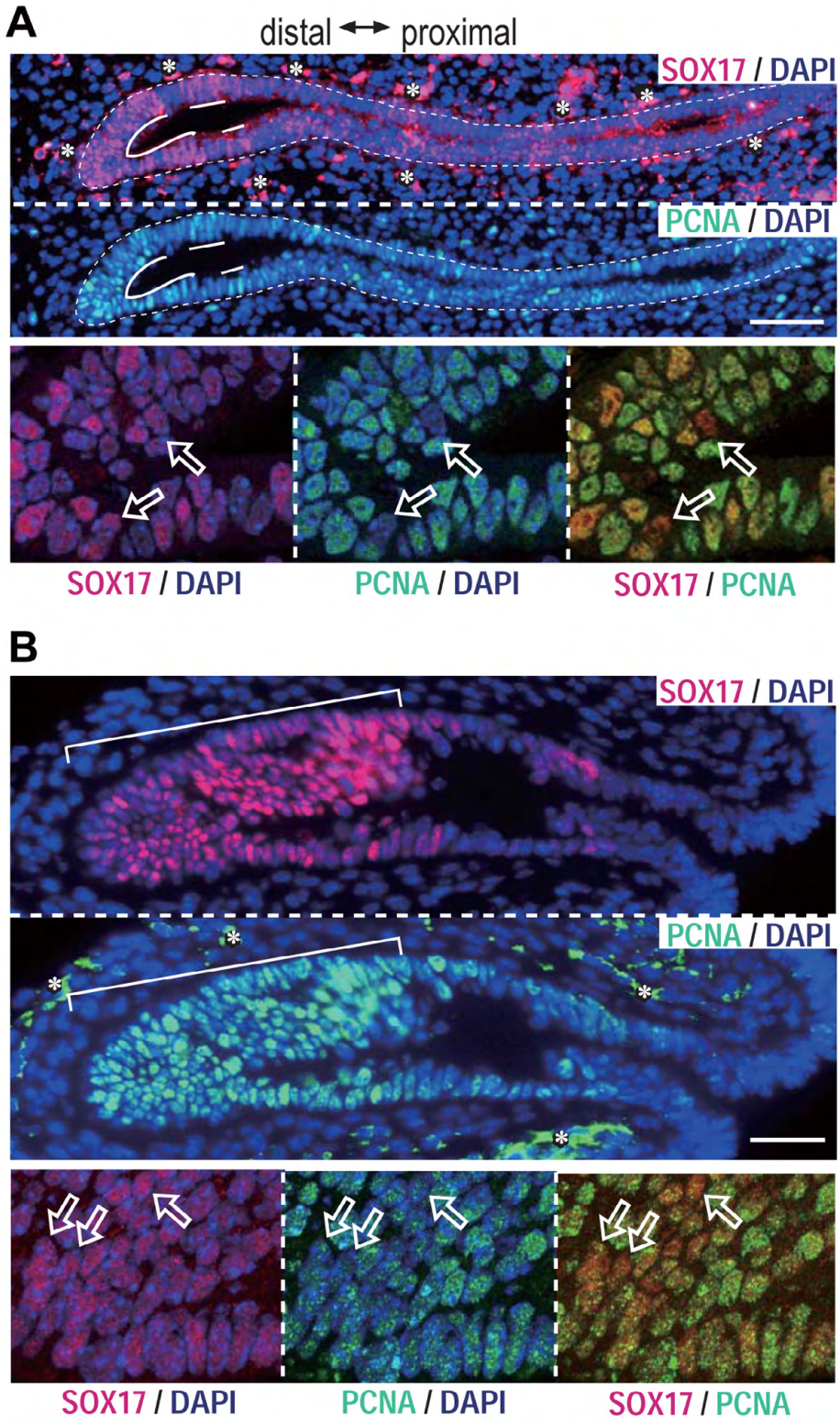

Fig. S4. Overlapping patterns of PCNA-positive and SOX17-positive domains in the bile duct epithelia of the gallbladder primordium *in vivo* and *in vitro*. (**A**,**B**) Anti-SOX17 (red fluorescence) and anti-PCNA (green fluorescence)-stained images showing the overlapping expression of SOX17/PCNA-positive domains (unbroken lines along the luminal surface in A; unbroken bars along the outer surface in B) in the gallbladder epithelial cells *in vivo* (15.5 dpc; A) and *in vitro* (a 3-day organ culture of gallbladder primordium initiated at 13.5 dpc; B). The Sox17- and PCNA-double positive cells appear to be enriched in the developing epithelial folds of the gallbladder explants. Arrows indicate SOX17-positive/PCNA-negative epithelial cells. asterisk, non-specific fluorescence in the red blood cells. Scale bar: 50 μm.

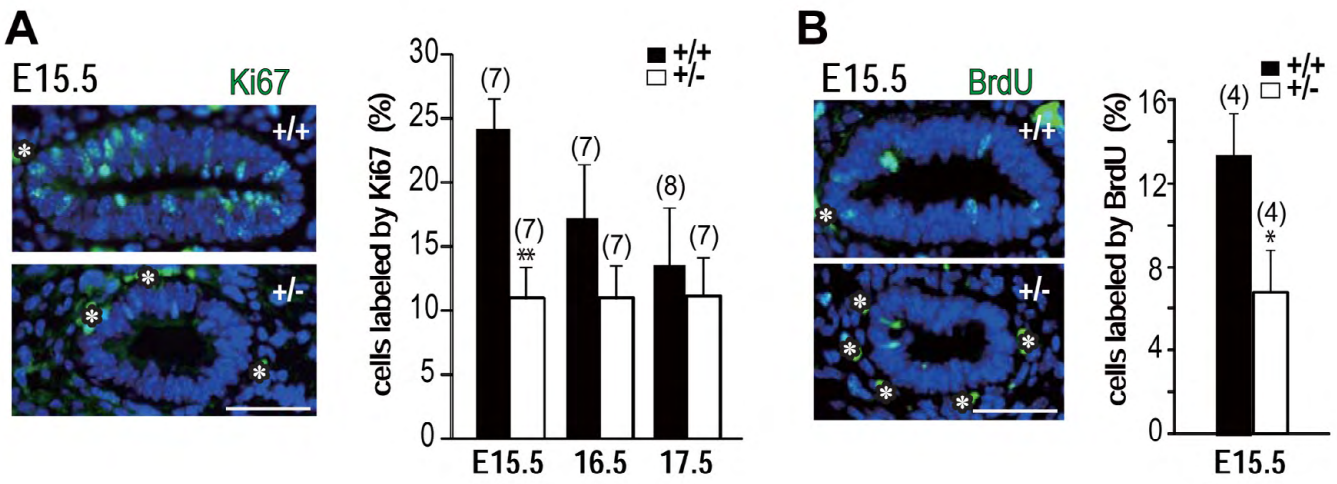

Fig. S5. Ki-67- and BrdU-labeling indices in *Sox17*$^{+/-}$ gallbladder epithelium at 15.5 to 17.5 dpc. (**A**,**B**) Anti-Ki-67 (A) and anti-BrdU (B) immunofluorescence images (left panels) and quantitative data (right graphs) showing significant reduction in both Ki-67-positive and BrdU-positive indices in *Sox17*$^{+/-}$ gallbladder epithelia at 15.5 dpc, compared with wild-type counterparts (**P<0.01 in A; *P<0.05 in B). Numbers in parentheses indicate the total number of embryos used in each group. asterisk, non-specific fluorescence in the red blood cells. Error bars represent s.e.m. Scale bar: 50 μm.

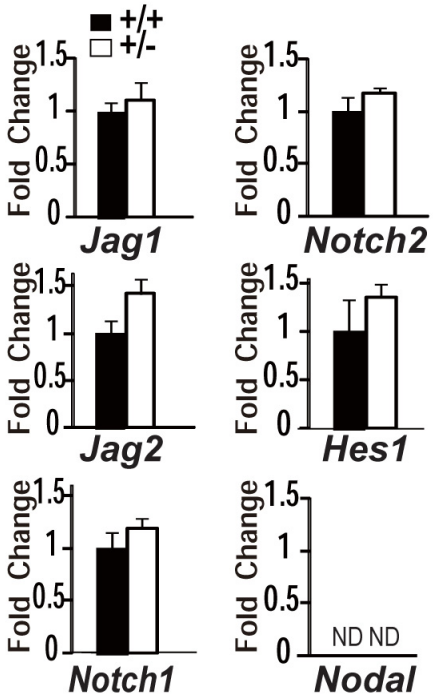

Fig. S6. No significant changes in the mRNA expression levels of notch and nodal signaling molecules in the gallbladder primordium. Real-time RT-PCR analysis showing no significant differences in mRNA expression levels of *Jag1*, *Jag2*, *Notch1*, *Notch2, Hes1* and *Nodal* between wild-type and *Sox17*$^{+/-}$ gallbladder primordia at 15.5 dpc (the mean value of wild-type gallbladder was set as 1). *Nodal* expression was undetectable in both genotypes. Error bars represent s.e.m.

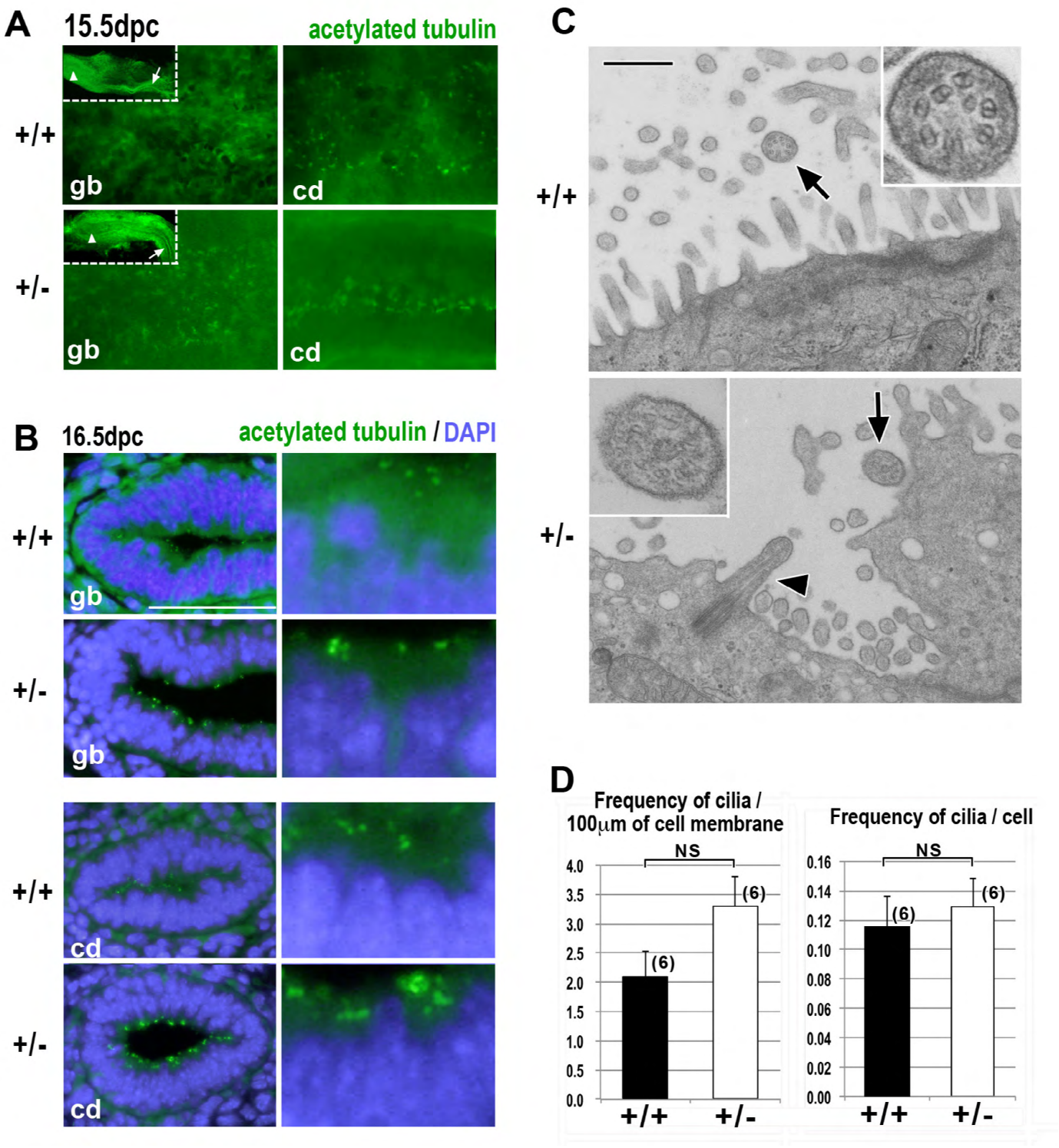

Fig. S7. No appreciable defects in distribution and frequency of primary cilia in the gallbladder and bile duct system in the *Sox17*$^{+/-}$ B6 embryos. (**A**,**B**) Whole-mount (A) and section (B) anti-acetylated tubulin staining of the gallbladder/ bile duct in wild-type and *Sox17*$^{+/-}$ B6 embryos at 15.5 and 16.5 dpc. No appreciable defects in the distribution patterns of primary cilia are found on the apical surface of the epithelial cells of *Sox17*$^{+/-}$ gallbladder (gb) and cystic duct (cd) regions. In the gallbladder region, the frequency of anti-acetylated tubulin-positive deposits appears to be increased, rather than reduced, compared with that in wild-type counterparts. In A, the insets show lower magnified images of the stained samples, in which arrowheads and arrows show the gallbladder and cystic duct regions, respectively. (**C**,**D**) Electron microscopic images (C) and quantitative data (D) showing proper formation of the primary cilia in the *Sox17*$^{+/-}$ gallbladder epithelia at 16.5 dpc. The frequency of the primary cilia per length of apical surface membrane (left graph) appears to be increased (P=0.052), rather than decreased, in the *Sox17*$^{+/-}$ gallbladder epithelia, although there were no differences in cilia frequency per cell between two genotypes (right graph). Numbers in parentheses indicate the total number of embryos used in each group. In C, the arrowhead and arrows show the sagittal and transverse (insets) images of the primary cilia, respectively. cd, cystic duct; gb, gallbladder. Error bars represent s.e.m. Scale bars: 50 μm in A,B; 0.5 μm in C.

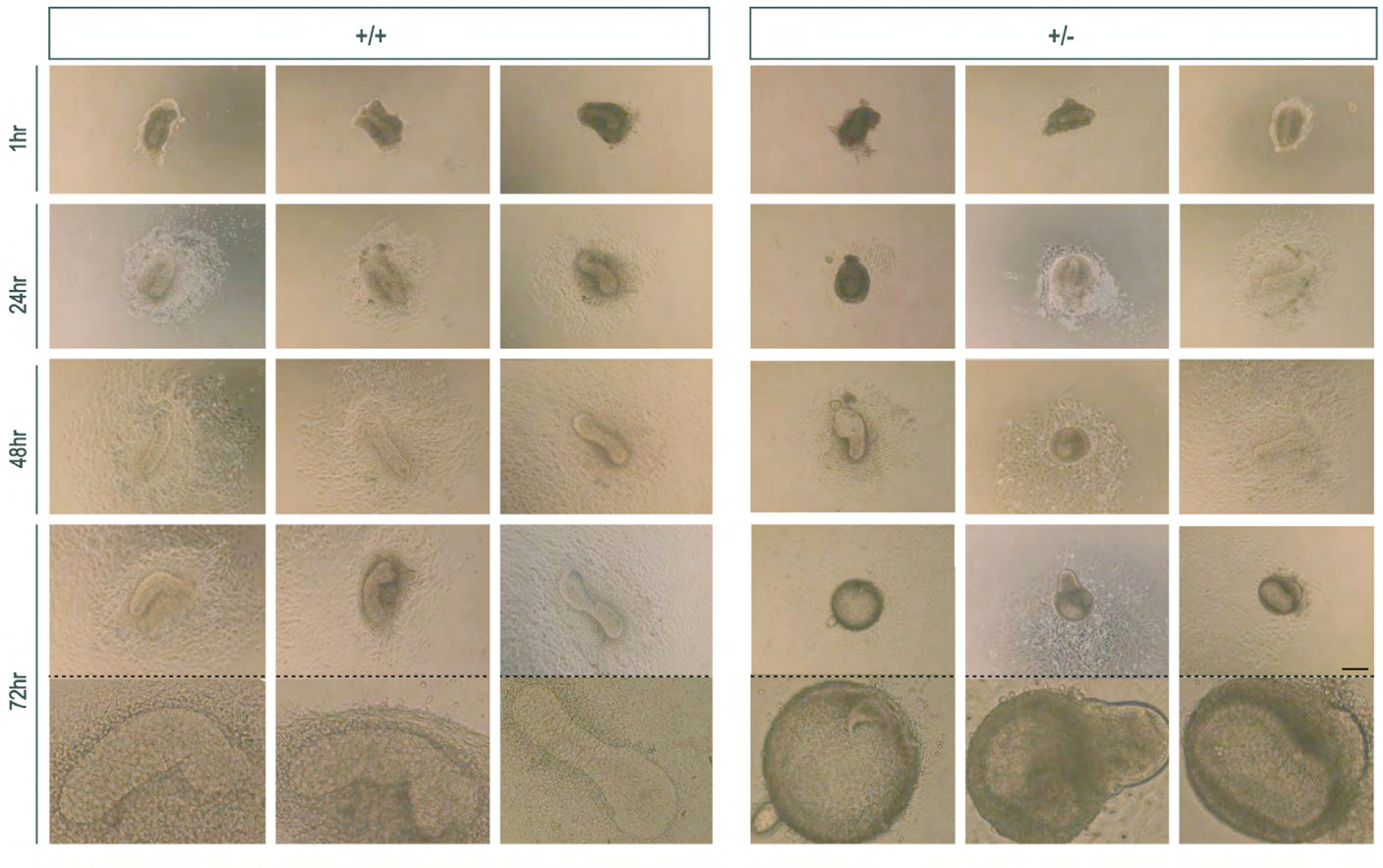

Fig. S8. Phase-contrast images of the time course of 3-day organ culture of the gallbladder primordium initiated at 13.5 dpc. Gallbladder primordia were isolated from *Sox17*$^{+/-}$ and wild-type littermates, placed on gelatin-coated plates, and then cultured in 10% fetal calf serum-DMEM at 37°C for 72 hours. In each explant, the phase-contrast images of the time course were acquired by hand with only a short culture interruption. Scale bar: 200 μm.

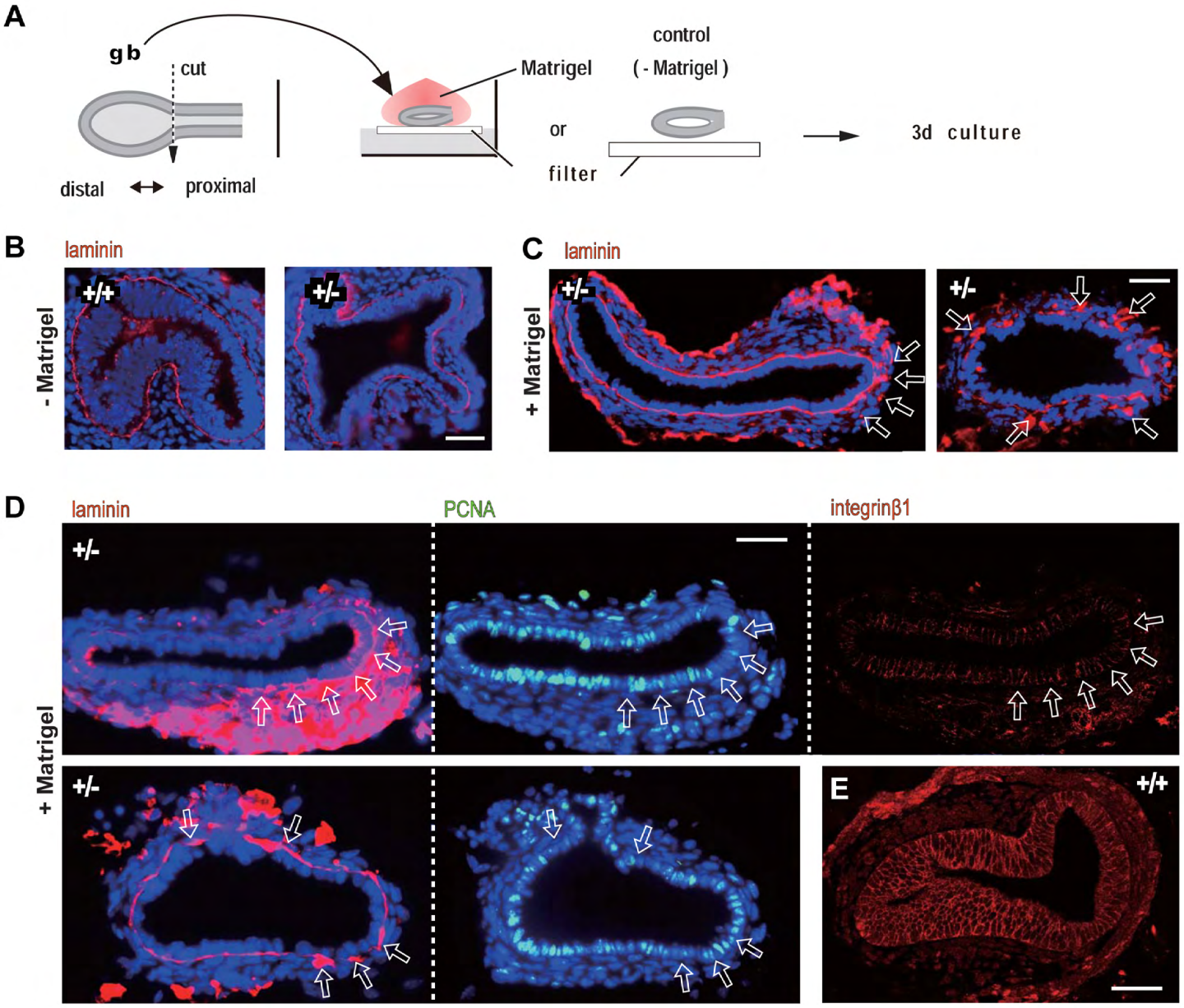

Fig. S9. Exogenous supply of basement membrane matrix (Matrigel) is not able to rescue the defects in the epithelial morphogenesis and polarized proliferation in the *Sox17*$^{+/-}$ gallbladder primordia *in vitro*. (**A**) A schematic showing the organ culture experiment of the 13.5-dpc gallbladder explants embedded in Matrigel on the filter (3 days). All gallbladder tissues were punched by a 27G needle in the presence of Matrigel before the culture initiation. (**B**) Anti-laminin staining of the control explants (in the absence of Matrigel) showing endogenous laminin distribution in the wild-type and *Sox17*$^{+/-}$ gallbladder explants. (**C**,**D**) Anti-laminin staining of the *Sox17*$^{+/-}$ gallbladder explants embedded in Matrigel, showing various distribution patterns of exogenous basement membrane matrix (C,D, arrows) around the *Sox17*$^{+/-}$ gallbladder epithelial cell layer. However, almost all of the gallbladder epithelial cells display a single cuboidal epithelial layer irrespective of whether they were directly underlined by exogenous basement membrane matrix or not. Anti-PCNA and integrin β1-stained images also show no appreciable differences in PCNA-positive domains and reduced integrin β1 expression between the epithelial cells with or without direct contact of the exogenous basement membrane matrix. (E) Anti-integrin β1 staining image of the wild-type (control) gallbladder explant. Scale bar: 50 μm.

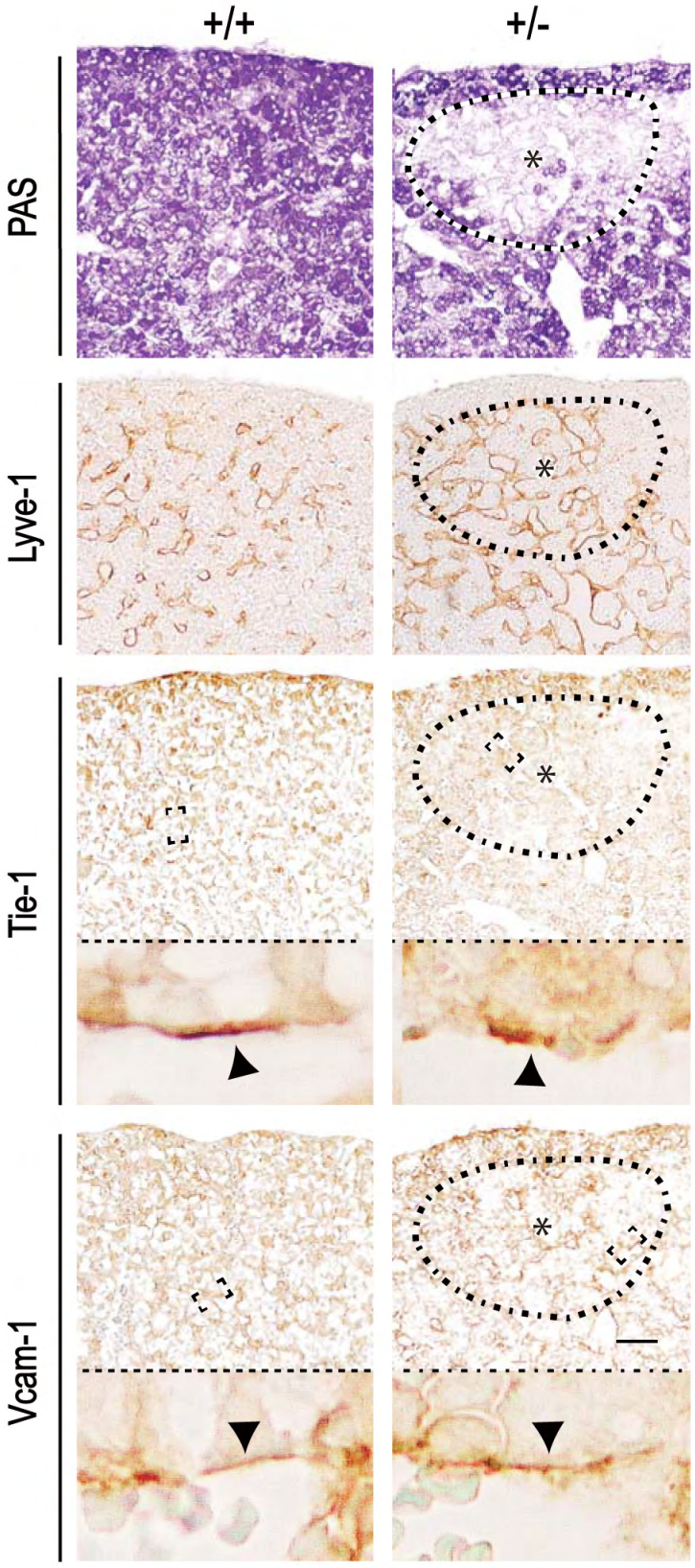

Fig. S10. No appreciable defects in the liver vasculature network of *Sox17*$^{+/-}$ livers at 17.5 dpc. Immunohistochemical analysis of continuous serial sections showing no appreciable differences in the immunoreactive expression of Lyve-1, Tie-1 and Vcam-1 in vascular endothelial cells (arrowheads) between wild-type and *Sox17*$^{+/-}$ livers (even in the degenerative region of *Sox17*$^{+/-}$ livers). The insets indicate higher-magnified images of the area surrounded by the broken rectangles in upper plates. Asterisks surrounded by dashed lines indicate degenerative regions. Scale bar: 50 μm.

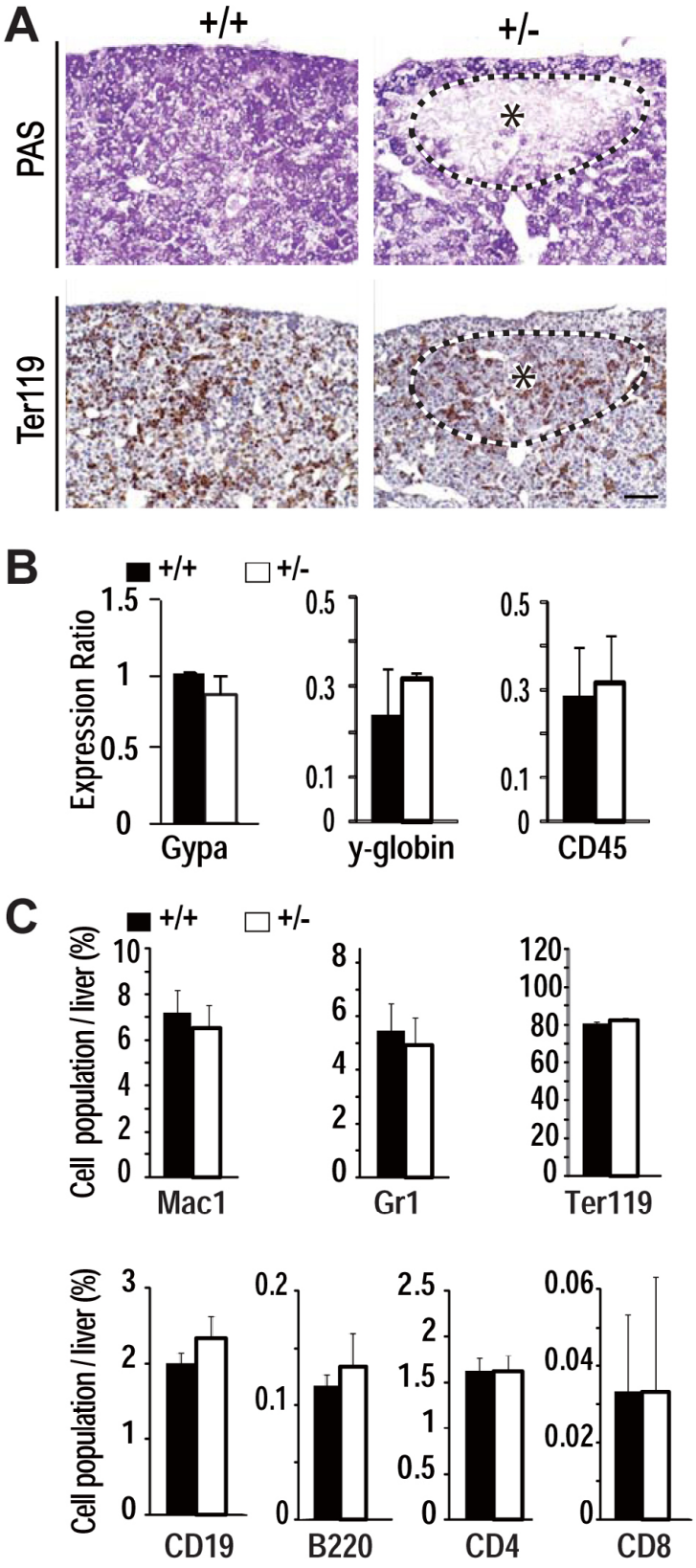

Fig. S11. No appreciable defects in hematopoietic cells of *Sox17*$^{+/-}$ livers at 17.5 dpc. (**A**) Immunohistochemical staining of serial sections showing no appreciable changes in the distribution of Ter119-positive hematopoietic cells, even in degenerative regions of *Sox17*$^{+/-}$ livers. Asterisks surrounded by dashed lines indicate degenerative regions. (**B**) Real-time RT-PCR analysis showing no significant changes in the mRNA expression levels of Gypa, Y-globin and CD45 between wild-type and *Sox17*$^{+/-}$ livers (n=4 in each). (**C**) Flow cytometric analysis using various markers specific for myeloid (Mac-1, Gr-1), erythroid (Ter119), B-lymphocytes (CD19, B220) and T-lymphocytes (CD4, CD8), showing no appreciable differences in each hematopoietic cell population between the wild-type (n=6) and *Sox17*$^{+/-}$ (n=3) livers. Scale bar: 50 μm.

Table S1. Seventeen downregulated genes in *Sox17*$^{+/-}$ livers with severe and mild phenotypes of *Sox17* heterozygote (B6) embryos compared with wild-type littermates at 17.0 dpc*

Description	Gene	Fold change‡	
		Severe	(Mild)
betaine-homocysteine methyltransferase	*Bhmt*	–5.7	(–2.8)
aldo-keto reductase family 1, member D1	*Akr1d1*	–4.9	(–3.2)
carbonic anhydrase 3	*Car3*	–4.9	(–3.0)
complement component 9	*C9*	–3.7	(–2.6)
cytochrome P450, family 7, subfamily a, polypeptide 1	*Cyp7a1*	–3.2	(–2.1)
carboxylesterase 3D	*Ces3d*	–3.2	(–3.2)
cytochrome P450, family 2, subfamily f, polypeptide 2	*Cyp2f2*	–3.2	(–3.0)
ectonucleotide pyrophosphatase/phosphodiesterase 3	*Enpp3*	–2.8	(–2.6)
cytochrome P450, family 3, subfamily a, polypeptide 11	*Cyp3a11*	–2.6	(–2.0)
alanine-glyoxylate aminotransferase 2-like 1	*Agxt2l1*	–2.5	(–2.3)
RIKEN cDNA C730007P19 gene (sulfotransferase family 2A, dehydroepiandrosterone (DHEA)-preferring, member 2)	*C730007 P19Rik* (*Sult2a2*)	–2.5	(–3.7)
SPARC related modular calcium binding 2	*Smoc2*	–2.5	(–2.0)
gelsolin	*Gsn*	–2.5	(–2.0)
predicted gene 7969	*Gm7969*	–2.3	(–3.0)
GLE1 RNA export mediator (yeast)	*Gle1*	–2.3	(–2.0)
solute carrier family 22 (organic anion transporter), member 8	*Slc22a8*	–2.0	(–2.1)
expressed sequence AI317395	*AI317395*	–2.0	(–2.0)

*Microarray expression analyses were performed using the cDNA samples collected from the central proximal region of the liver lobules in which any degenerative area was detected based on gross anatomy, even in the severe group. In the mild group, the cDNA samples were also prepared from the proximal regions of the liver lobules.

‡The fold change represents the difference in expression levels in livers between *Sox17*$^{+/-}$ and wild-type littermates. Differential expression was defined as a difference of twofold or more.